FLUID STRUCTURE INTERACTION IN HIGH PERFORMANCE CATAMARAN C-FOILS UNDER LOAD

L. Marimon Giovannetti[1], L.Marimon-Giovannetti@soton.ac.uk, **J. Banks**[2], J.Banks@soton.ac.uk, **S.W. Boyd**[3], S.W.Boyd@soton.ac.uk, **S.R. Turnock**[4], S.R.Turnock@soton.ac.uk

Abstract. An experimental technique to accurately quantify the deformation and the bend-twist coupling of high performance composite foils under fluid loading is presented. The experimental results are reproduced in a Computational Fluid Dynamic (CFD) environment to assess the impact of board deflection and changes in pitch angle on vertical force generated in the C-foils while sailing under increased hydrodynamic pressure.
A three dimensional Digital Image Correlation (DIC) methodology suitable for use within a wind tunnel is developed. The technique allows for the measurement of full-field deflection during fluid-structure interaction (FSI) experiments. Combined with DIC technique, the C-foil tip vortex is investigated using Particle Image Velocimetry (PIV) to correlate the variation of the vortex position and strength to the deflection of the board. These techniques, combined with CFD investigations allow potential changes in structural behaviour to be assessed with regard to improving the performances of the foils in sailing conditions.
Experimental results are presented for a high performance curved foil from a NACRA F20 catamaran tested within the University of Southampton RJ Mitchell wind tunnel. The fluid regime is chosen to have a Reynolds number equivalent to light upwind sailing conditions ($Rn=6.66x10^5$: boat speed of 6 knots) with a fifth of the fluid loading experienced in the water. Curved foils provide both a hydrodynamic side-force to counteract the aerodynamic forces of the sails and a vertical lift force to reduce the wetted surface area and hence the resistance. It is therefore necessary to investigate from a sailor point of view the influences of the side force and vertical coefficients that the change in effective angle of attack and of pitch will give to the stability and the performances of the catamaran.

NOMENCLATURE

AoA	Angle of Attack [deg]
C_D	Drag Coefficient
CFD	Computational Fluid Dynamics
C_L	Side Force Coefficient
C_Z	Vertical Coefficient
DIC	Digital Image Correlation
FEA	Finite Element Analysis
FSI	Fluid Structure Interaction
F_L	Lift force in wind tunnel axis [N]
F_x	Drag force in board axis [N]
F_y	Sideforce in board axis [N]
PIV	Particle Image Velocimetry
r	radius [m]
R_n	Reynolds number
V_S	Wind speed [$m.s^{-1}$]
δ	Deflection [mm]
θ	Twist angle [deg]
ν	Kinematic viscosity of fluid [$m.s^{-1}$]
ρ	Density of fluid [$kg.m^{-3}$]
φ	Pitch angle [deg]
ψ	Stereo angle [deg]

1. INTRODUCTION

The present research addresses experimental and numerical approaches related to the evaluation of bend-twist elastic coupling in high performance sailing catamarans daggeboards. NACRA Performance sailing has produced two high performance catamarans in the last five years. The NACRA F20c sails in the F20 class with a heavy weight male crew and the NACRA 17 that was chosen in 2012 over a wide range of other catamarans as being the new mixed gender class in the next Olympic event, in Rio 2016. Both of these present two C-foils daggerboards. This configuration permits them to sail in a normal catamaran configuration (i.e. the leeward hull in the water and the windward hull off the water) and in a foiling configuration. The foiling configuration, which implies the boat is "flying" with both hulls above the water, greatly reduces the wetted area of the hulls. Therefore, for the crew it is necessary to enhance this condition in order to improve the performance. The strict regulations of Olympic classes [1] do not permit active devices to change the angle of attack of the C-foil while sailing, however they permit to enclose the foils in the daggerboard case changing the incidence angle, slightly controlling the angle of attack and the angle of pitch. It is therefore necessary to understand the structural behaviour under fluid loading of the foils in order to enhance the foiling configuration in increased hydrodynamic conditions (i.e. foiling downwind). The possibility of controlling the effective angle of attack, in both leeway and pitch direction, of the C-foils tailoring the structure might benefit the sailors as they should be able to foil more comfortably and for longer periods in downwind conditions.

The research investigated the effects of the C-foil structure under aerodynamic loadings in the 11'x8' R.J. Mitchell wind tunnel with the aid of three dimensional DIC. This technique involves the use of digital cameras that register a series of images of a surface on which a randomised speckle pattern is applied. The key advantages are the use of simple equipment (i.e. cameras, lenses, lights and a computer), the fact that it is a non-

1 PhD Student, University of Southampton, Fluid Structures Interaction Group
2 Research Fellow, University of Southampton, Fluid Structures Interaction Group
3 Associate Professor, University of Southampton, Fluid Structures Interaction Group
4 Professor, University of Southampton, Fluid Structures Interaction Group

contact measurement and its high fidelity of precision, [2]. Within DIC software, the speckle pattern is mapped to calculate the deformed shape, thereby allowing the derivation of the deflections and strains of the investigated object, [3]. The use of two cameras, in a stereo configuration, allows for the measurement of deformations both in the plane normal to the camera and out of plane, i.e. 3D DIC. This technique, can also describe the shape of the investigated specimen. The possibility of investigating the shape deformation is necessary to study the influences in the changes of the effective angle of attack. For 3D DIC the angle between the cameras controls the measurement accuracy of the out of plane deformation [2, 3, 4, 5]. Therefore optimizing the stereo angle between the two cameras for out of plane accuracy is essential [5, 6, 7]. DIC has been widely used and validated for two-dimensional and three-dimensional analysis of small specimens, [2, 3, 8]. These are mostly analysed using small stereo angles (ψ up to 17°) as this increases the in-plane resolution [5, 7]. Three-dimensional DIC for a wide range of stereo angles and lenses are presented by Ke et al. and Phillip Reu, [7, 5], and deflections and strains are assessed with experimental values, showing the possibility of increasing the stereo angle up to ψ =60° for large out of plane deformations.

A fluid structures interaction experiment was possible coupling PIV with DIC. PIV is also a full-field non-contact technique that describes the flow field surrounding an object measuring the flow velocities in the *x* and *y* direction, *u* and *v* respectively. Two images are taken of particles moving through a thin laser sheet, allowing the particle displacement, and therefore the velocity, to be calculated [9].

The present research aims to develop a methodology that accurately captures the passive deformation of a foil structure under a loading condition and the fluid behaviour surrounding it. Current FSI studies have been mostly focusing on numerical techniques to model the structural deformation under fluid loading utilising FEA and CFD [10, 11, 12, 13]. Taking the two techniques in isolation, there are a variety of methods that validate the numerical models.

However, the developed approach that uses coupled 3D DIC and 2D PIV allowed the evaluation of a complete FSI experimental methodology. The two techniques are coupled in the overall fluid structure interaction experiment as both are recording simultaneously to the applied wind, but the systems are isolated between each other employing the use of camera filters and coloured gels that ensure separation between the white light imaging technique (i.e. DIC) and the laser-based PIV. The experimental deflection results are then replicated in CFD simulations to assess the validity of the numerical model and to allow other conditions to be investigated such as increased deflection due to hydrodynamic loading in water and different pitch angles, not investigated in the wind tunnel.

The present project aims to investigate how board deflection and foil orientation affect the vertical force generated allowing the catamaran to maintain a foiling configuration as long as possible, minimising the wetted surface area.

2. EXPERIMENTAL SETUP

The experiments were conducted in the 3.5 m x 2.4 m RJ Mitchell wind tunnel at the University of Southampton. This closed circuit tunnel operates at wind speeds of 4 to 40 ms^{-1} with turbulence levels less than 0.2%. The aerodynamic forces on the NACRA F20 C-foil are calculated with a six component Nutem load cell balance, mounted on a turntable in the tunnel roof. The forces and moments are measured in the turntable axis system about the wind tunnel balance centre 1.27 m below the tunnel roof. The aerodynamic data were acquired using a sampling frequency of 1 kHz over a period of 10 seconds. Repeats were acquired in order to assess the repeatability and robustness of the aerodynamic and structural results. Figure 1 shows the dynamometer and C-foil arrangement within the cross-section of the wind tunnel.

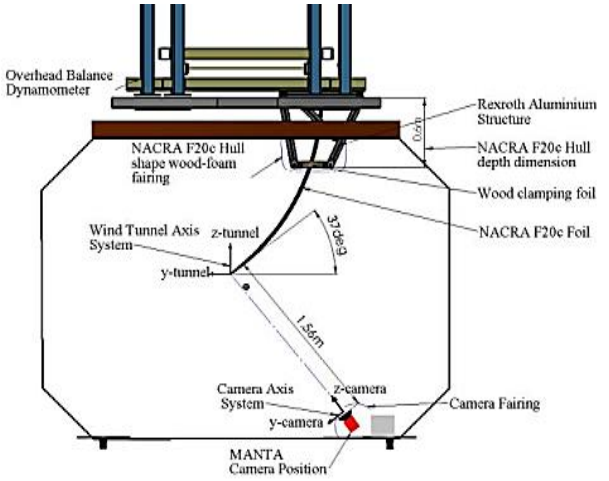

Figure 1: Wind tunnel working section diagram showing dimensions, dynamometer and C-foil mounting system.

The Nuntem balance was calibrated applying known static loads to a pulley system normal to the C-foil and acquiring a new zero value before and after each aerodynamic run.

Figure 2 shows the NACRA F20 daggerboard under investigation. The shape and projected area dimensions are reported. The root outer-shape section is symmetrical and curves toward the tip with a curvature radius r~ 2.85m, tapering the leading edge in the three-dimensions in the bottom 18%.

In the experiments AoA=0° is set in the condition at which the lift force is zero. The lift force is defined in tunnel axis system as:

$$F_L = F_x \cos(AoA) - F_y \sin(AoA) \quad (1)$$

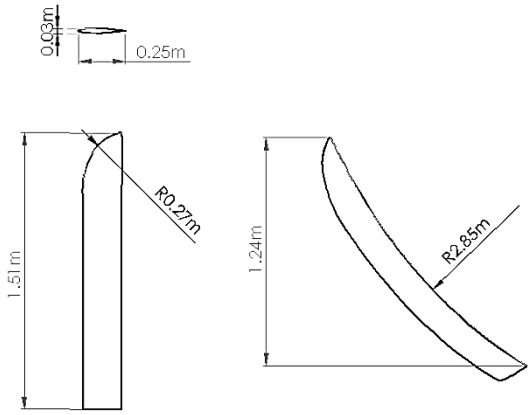

Figure 2: NACRA F20 daggerboard: projected area, shape and dimensions.

2.1 DIC set-up

A stereo DIC system was set up in the wind tunnel. It allowed to detect the in-plane and out-of-plane deflections of tip of the C-foil, within a 0.3x0.3 m field of view. The sampling frequency of the cameras was set at 1Hz, so that only steady deflections could be calculated. The frequency is set to comply with the cameras specifications. All the tested conditions were recorded for 30 seconds (i.e. 30 images) and were repeated in two sets and two days of testing to provide confidence in the repeatability of the results. In the experiments the DIC cameras were connected to one spare channel of the balance to record the exact aerodynamic force per image. The DIC random speckle pattern size and density was chosen to minimise the errors within a range of deflections between 0.5 to 20 mm [14]. The speckle pattern was created using the program ImageJ and represents a speckle size of approximately 6.3 pixels. It was applied on the C-foil with Decal paper. The accuracy of the DIC system in the wind tunnel environment was assessed moving an airfoil-shape section by known amount with Vernier scale micrometre with accuracy of $1/20^{th}$ mm. The maximum percentage error recorded was <2.5% for applied displacements of 0.5-1mm and <1% for applied displacements of 2-20mm [14]. The equipment used is described in Table 1.

Table 1: DIC performance table

Equipment Item	Set-up
Camera	2MANTA G-504B/C Sensor size : 8.5x7.1 mm Pixel size: 3.45 µm Resolution (max): 2452x2056 pixels Magnification: 0.15 Exposure time 3500-8000 µs Frame rate: 1Hz
Lens	Nikon: Nikkor 50mm f/1.8 D Aperture: f-11
Light	1x8 high power LED light source 2xNILA Zaila LED
Speckle pattern	Speckle size: ~6.3 pixels Dimensions: 250x270 mm

Prior to the experiment, an assessment on the resulting field of view was made in order to comply with the constrained dimensions of the wind tunnel and the deflection of the board. A stereo angle of ψ =45° was chosen to maximise the resolution of the out-of plane deflection whilst minimising the in-plane displacement errors and allowing a 25° range in angle of attack without moving the DIC equipment. Therefore, the equipment was chosen to allow a depth of field of ~ 180mm.

2.2 PIV set-up

As for the DIC, it was extremely important to pay particular care in the set-up of the experiment. 2D PIV was used to calculate the vortex strength and position, implying the use of one camera, lens and one green laser. The PIV sensor camera was placed within the wind tunnel, downstream of the NACRA F20 board. The laser was positioned in the viewing room pointing its sheet one chord aft the foil's tip across the wind tunnel. This position permits to capture the vortex position and its shift with tip-displacement (calculated with DIC). Figure 3 shows the schematic diagram of the position of the PIV equipment within the working section of the wind tunnel.

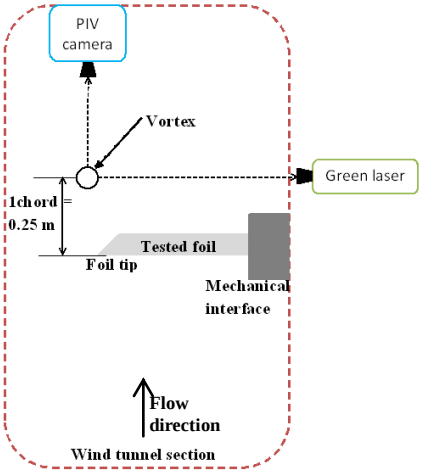

Figure 3: PIV set-up diagram within the R.J. Mitchell wind tunnel to capture the vortex strength.

Seeding particles were introduced into the tunnel using a smoke machine on a timer. The time between the two image frames was set to ensure that the majority of the particles were observed in both frames, avoiding saturation of seeding particles. The images were captured in cross-correlation therefore the scattered light from the first and second exposure of the seeding particles was recorded in two different images.

During the set-up it was extremely important for the laser sheet to be perpendicular with respect to the flow velocity and the camera position, to avoid spurious velocity angles that would decrease the accuracy of the results. In order to obtain a sharp enough laser sheet at the vortex location appropriate optics were applied to the laser orifice, to produce the required sheet thickness approximately 2 m away from the laser outlet. The final thickness at maximum power was detected as being 4 mm at the vortex location. Table 2 describes the equipment used on the PIV experiments.

Both DIC and PIV results were processed using the LaVision Software DaVis.

Table 2: PIV performance table

Equipment Item	Set-up
Camera	PowerView Plus 4MP model 630059 Sensor size : 15.15x15.15 mm Pixel size: 7.4 µm Resolution (max): 2048x2048 pixels Intensity dynamic range: 12 bit Operation mode: triggered ΔT: 100, 50, 30 and 20µs for V_S=10,20,30 and 40 ms^{-1}
Lens	Nikon 200mm f/4 AF-D Aperture: f-4
Laser	Quantel Twins BSL 200 green laser Wavelength: 532 nm Energy per pulse: 200 mJ

3. EXPERIMENTAL RESULTS

3.1 Aerodynamic forces

The fluid dynamic forces recorded by the overhead balance were converted into tunnel axis system based on the yaw angle of the dynamometer. The side force, drag and vertical force coefficients (i.e. C_Y, C_D, and C_Z respectively) were therefore calculated. It was possible to analyse the response of the NACRA F20 daggerboard for a complete range of angles of attack and two wind speeds. The side force coefficient is shown in Figure 4. It is possible to see that stall occurs at AoA=13.5°. The post-stall condition shows, as expected, a drop in lift and vertical coefficients and an increase in drag. However, the maximum side force and vertical force coefficients in separated flow increase while increasing the wind speed, contrarily the drag decreases, This variation in the coefficients can be explained either by the Reynolds number affecting the flow separation or by the board deflection twisting toward feather (i.e. decreasing AoA of approximately 1°). The twist phenomenon is possible as the torsional axis is positioned upstream of the aerodynamic centre of effort. The larger variation in the post stall condition is also affected by a shift of the centre of effort toward the trailing edge of the foil (from 28% to 40% of the chord), creating more separation between the torsional shear centre and the centre of pressure points [14].

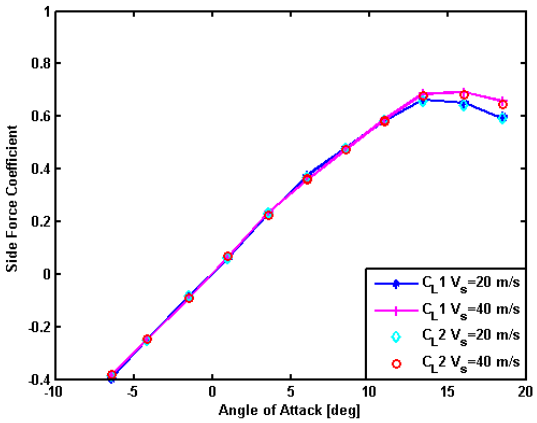

Figure 4: Lift coefficient over angle of attack aerodynamic sweep under two wind conditions.

Analysing the time history of the forces it was possible to assess the first resonant frequency of the board as being 18Hz. Large variations were encountered in the vertical force component, due to the curved nature of the Foil. As the tip oscillates up and down the apparent angle of attack of the flow varies, causing large oscillations in the vertical force generated near the tip.

3.2 Structural response to fluid loads

The deflections, averaged over 30 images for each condition, in the *x*, *y* and *z* direction are calculated using the DIC system. The tip deflection magnitude for each representative wind speed (V_S= 20, 30 and 40ms^{-1}) and angle of attack (AoA ~ 0, 3.5, 8.5, 13.5 and 18.5 degrees) is calculated for both set of tests. Figure 5 shows the DIC displacement results compared to the force normal to a plane passing though the root and the tip of the board for two repeats of the experiment. The deflection shows a linear increase with respect to the normal force applied. Moreover, it can be seen an increase in standard deviation proportional to the increase in wind speed and angle of attack (and hence aerodynamic force).

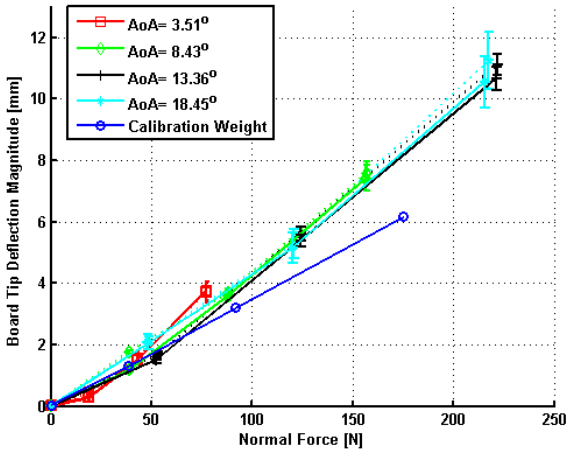

Figure 5: Tip displacement magnitude calculated with DIC at different aerodynamic force magnitudes for two repeats (i.e. mean deflection from the first set of images displayed as solid line and second set displayed as dotted line) showing the standard deviation of the results.

The variation of the tip displacement greatly increases for the high angles of attack and wind speeds, showing that despite the low acquisition rate, the dynamic motion of the board can be identified. In order to accurately assess the dynamic displacements, future tests will be performed with high speed DIC cameras.

The results show an excellent repeatability and robustness. The DIC results are also measured for a known static load case, which present a linear increase in deflection with increased weight. The difference in slope between the static and the dynamic test derives from the change in centre of effort from a single point load to a dynamic pressure distribution, as the static load is applied to the approximated static centre of effort.
It has to be noted that the fluid forces in air are significantly lower than the ones experienced in water, therefore the measured deflections are smaller than those expected in the investigated sailing conditions.

In order to assess the effects of deflection on the leeway and pitch angles, the change in angle of attack was calculated. The out of plane deflection was calculated along lines running perpendicular to the trailing edge. The total chord length (i.e. 180, 150 and 80mm respectively from the top to the bottom at 80%, 88%, 97% of the span considered from the bottom of the hull) and the difference in out of plane deflection at the leading and trailing edges were used to calculate the local change in AoA. Figure 6 shows the change in twist with increased wind speed and angle of attack for the tip of the blade.

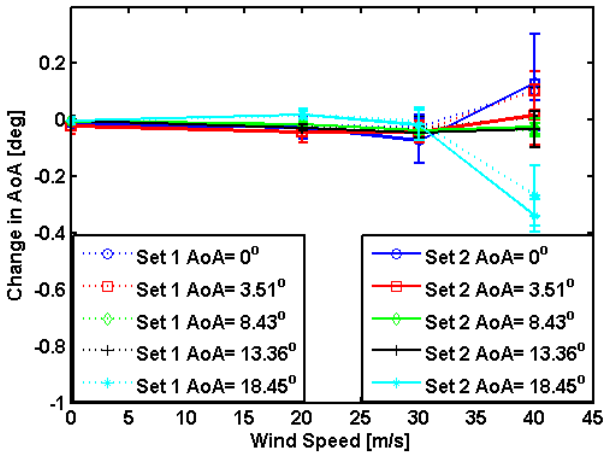

Figure 6: Twist angle over wind speed at 97% of the span.

From the figure, it can be seen that the effective angle of attack is decreased toward feather for high flow speeds and angles. The observed variation in twist near the tip could have a noticeable effect of the vertical force generated by the structure as small changes in local angle of attack can change the lift generated significantly. The figure shows a trend of positive change in twist for small angles of attack and a negative change in angle (i.e. toward feather) for large angles of attack. This non-linear trend is also observed in more flexible structures investigated, showing, not only the effect of the structure, but also the influence of the dynamic centre of effort, proving the efficiency of assessing the whole FSI environment. The decrease in effective angle of attack occurring in stall condition can be linked to the increase in lift and vertical coefficients with high wind speeds (Figure 4), showing the possibility to design the structures to control their behaviour in increased aerodynamic pressures. The small change in twist experienced in air does not affect greatly the aerodynamic response, also due to the stiffness of the investigated daggerboard. However, the non-linear response that is seen in the wind tunnel in increased loading condition (i.e. high wind speeds and angles of attack) might affect the flow while sailing. Therefore, more studies need to be performed to capture the response of twist to high loads.

3.2 Flow field measurements

For the PIV measurements, two angles of attack, namely AoA=8.5° and 18.5°, were investigated at a range of wind speeds. Both strength and position of the tip vortex are assessed. The vortex position was found with the basic VORTFIND algorithm, presented in [15]. The algorithm ranks which vectors are closest to the vortex centre using criteria defined in [16]. The average position of the vortex is therefore calculated for the investigated conditions, as can be seen in Figure 7. Both the mean and distribution of the experimental tip vortex position can be seen for different wind speeds and angles of attack in Figure 7. The impact of flow separation on the variability of the vortex position can be seen as the AoA increases.

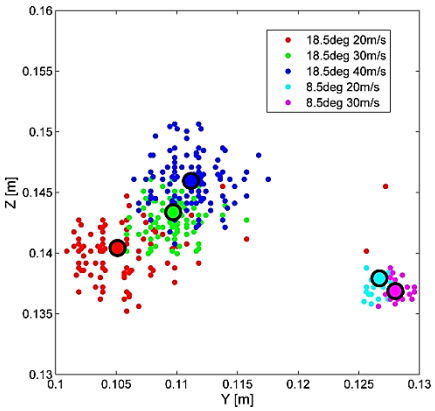

Figure 7: Tip vortex position for different wind speeds and angles of attack, with mean position highlighted in black.

From the figure it can clearly be seen that for high angles of attack the vortex centre changes its position (i.e. from the position at V_S=20 ms^{-1} to V_S=30 ms^{-1} it moves 6.5mm and at V_S=40 ms^{-1} it moves 10.5 mm). This phenomenon can be correlated to the tip deflection, as shown in Figure 5.

4. NUMERICAL RESULTS

Having conducted a set of experimental FSI tests, preliminary CFD results were produced in order to replicate the results obtained in the wind tunnel.
Initially the un-deformed C-foil daggerboard geometry was modelled with the hull fairings in a replicated wind tunnel fluid domain. Having assessed the validity of the numerical simulations, comparing the force coefficients with the experimental values and replicating the exact geometries and arrangement, the effects on board performances for small changes in deflections and pitch angle are investigated.

4.1 CFD simulations setup

In order to replicate the wind tunnel environment, a finite volume method for a single phase fluid was adopted.
This method is derived from the surface integration of the conservative form of Navier Stokes' equations over a control volume. The incompressible Reynolds averaged Navier- Stokes (RANS) equations, written in tensor form, are defined as

$$\rho\frac{\partial(U_i)}{\partial t}+\rho\frac{\partial(U_iU_j)}{\partial x_j}=-\frac{\partial P}{\partial x_i}+\frac{\partial}{\partial x_j}\left[\mu\left(\frac{\partial U_i}{\partial x_j}+\frac{\partial U_j}{\partial x_j}\right)\right]- \\ -\rho\frac{\partial}{\partial x_j}\left(\overline{u_i'u_j'}\right)+f_i \quad (2)$$

and

$$\frac{\partial U_i}{\partial x_i}=0 \quad (3)$$

for momentum and mass continuity respectively.
The effect of turbulence is represented in equation (2) by the Reynolds stress and is modelled using the k-omega SST turbulence model contained within OpenFOAM 2.2 [17].
A steady state solver was used, as can be seen in Table 3.

Table 3: Numerical simulations settings

Simulation item	Set-up
Type of mesh	Hexahedral (unstructured)
No. of elements	7-8 Milion
y^+ on the foil	1-60
Domain physics	R_n=6.6x10^5,5x10^5 and 3.3x10^5 k-ω SST fully tubulent model Automatic wall function
Inlet	Free-stream velocity 30 ms^{-1}
Outlet	Zero gradient
Bottom-side-top wall	Wall free stream velocity
C-foil and fairing	Wall no slip condition
Grad(U) scheme	Gauss linear
Div(U)	Gauss limited linear V1
Pressure coupling	SIMPLE
Convergence criteria	P=1e-7; U=1e-6; k= ω =1e-8

In order to correctly model the vortex strength and position, regions of mesh refinements were placed around the foil and in the estimated wake region, as can be seen in Figure 8.

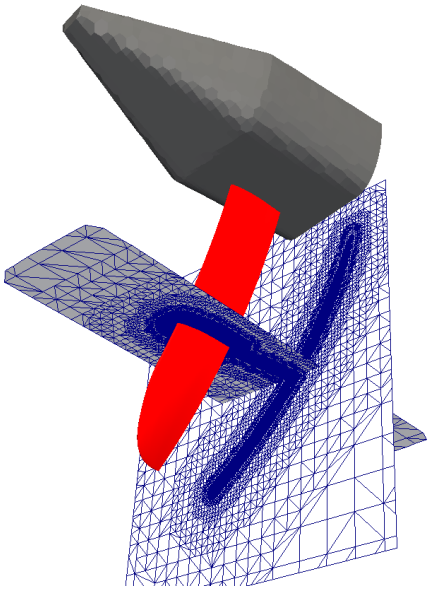

Figure 8: Mesh of C-foil with fairing

Two boundary layer elements are also grown out from the foil surface mesh.

4.2 CFD results

The force coefficients from the CFD results are compared with the experimental results for the V_S=30 ms^{-1} case. Figure 9 shows the tip vortex plane comparison between the CFD and the PIV results. Both figures include the board position as well as the vortex centre. The position of the vortex and its strength is further discussed in [18]. Figure 9 provides a qualitative comparison of the tip vortex position.

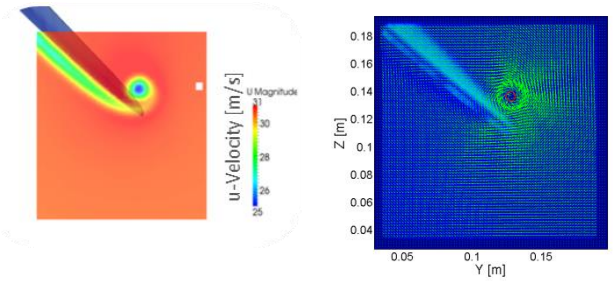

Figure 9: Flow field comparison for vortex strength and position between CFD results (left) and PIV experimental results (rigth)

In order to compare the CFD results with the experimental flow field data, the tangential velocity over the vortex centre position is presented in Figure 10. The experimental results show a very steep increase and decrease of the tangential velocity at the tip vortex that is not completely captured by the CFD model. This is mostly likely due to lack of mesh density in this region, therefore further mesh refinement in the laser sheet region will be performed. The large number of PIV data (i.e. 210 images per repeat) and the post-processing technique used (with overlap of 50% in the subsets) permits to reproduce very fine vector spacing that, in order to be reproduced by CFD models, requires a grid with spacing equal to the PIV spatial resolution.

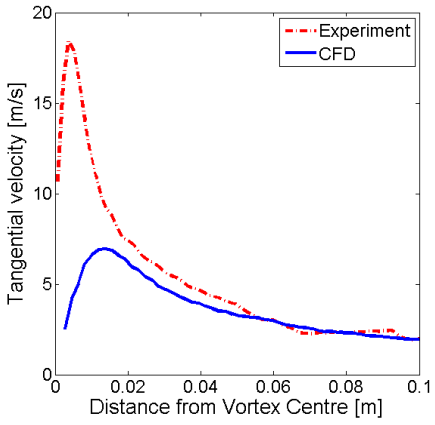

Figure 10: Mean tangential velocity at laser sheet position for AoA=8.5° and V_s=30 ms^{-1} over distance from the vortex centre

Considering initially only the un-deformed shape in the CFD simulations, a comparison of force coefficients is shown in Figure 11. It can be seen that the numerical results agree well for the lift and drag components for the pre-stall condition. It has to be noted that the simulations were steady state RANS, therefore, in order to correctly capture the post stall condition, transient simulations will be performed in future investigations. Moreover, the differences in vertical coefficients should be due to a slight misalignment in pitch angle of the daggerboard in the wind tunnel, with the inclusion of a small bow-up pitch angle.

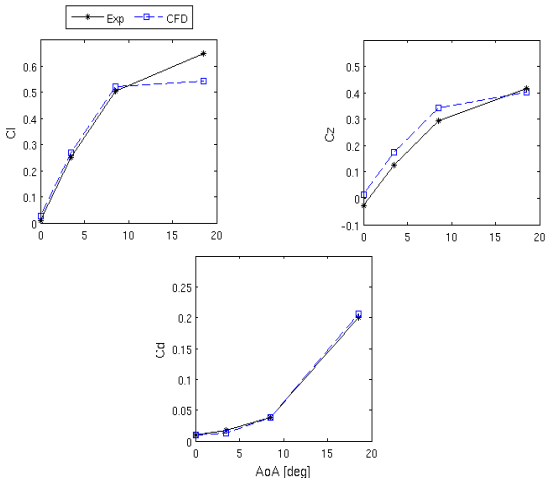

Figure 11: CFD and experimental force coefficients comparison

Having assessed the validity of the numerical simulations, the influence of pitch angle and pure deflection (with no twist) was taken into account. Figure 12 shows the change in force coefficient varying the pitch angle toward the inlet of the domain (bow up while sailing). The pitch variation was assessed with an applied angle of attack of AoA=8.5° and V_S=30 ms^{-1}. From the figure it can be seen the steep initial increase in force coefficients and the resultant stall occurring at φ=3°.
Furthermore, for the same conditions the influence in deflection was assessed. The deformed shape was created taking into consideration the in-plane and out-of-plane displacements from the DIC results and imported in the CFD simulations. The deflection magnitude measured in the wind tunnel for this condition is δ=3.78 mm.

In order to completely capture the effects of deflection in the responses of the C-Foil, an estimated deflection encountered in sailing conditions was also analysed. The sailing deflected shape was extrapolated considering the forces that would be experienced in water with a change in fluid density. This condition would correspond to $V_{s\ water}$=4.47 knots for a Reynolds number R_n=5x10^5.
Comparing the deformed geometry results with the initial numerical results, as shown in Figure 13, it was possible to outline a decrease in lift coefficient (with the foil deflecting toward the centre of the boat) and an increase in vertical coefficient. The drag coefficient presented a negligible change for both investigated shapes. Considering the lift and vertical coefficient of the un-deformed and the sailing condition shapes, the lift coefficient experiences a decrease of 4% and the vertical coefficient an increase of 2.85%.

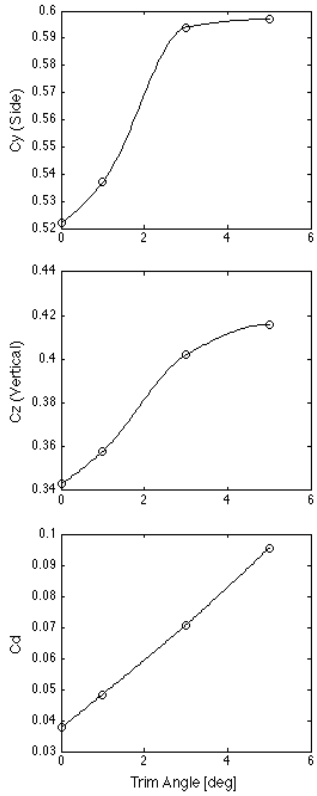

Figure 12: Force coefficients variation with pitch angle.

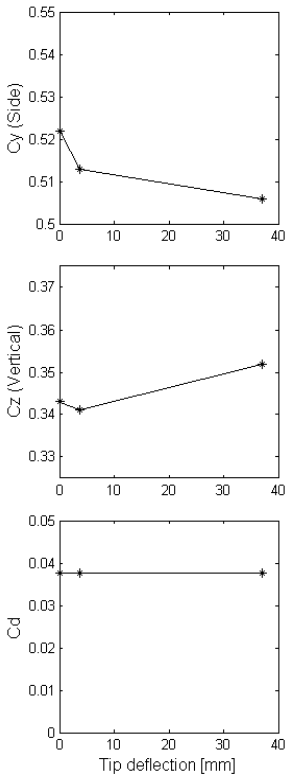

Figure 13: Change in force coefficients with tip deflection.

From the pitch and deflection investigations, it is possible to see that as the wind and boat speed increase, and the pitch angle increases, there is a rise in vertical force. However, when the C-Foil deflects a decrease in side force coefficients is noted. It is therefore necessary, while positioning the foils in the daggerboard cases, to find a compromise between side and vertical forces that can be ideal in flying condition. Moreover, whilst the deflection has no effect in the drag, the increase in pitch might be detrimental for the increased drag, if the hulls are not immediately lifted from the water.

5. CONCLUSIONS

During the study, a Fluid Structures Interactions experimental methodology has been developed and assessed. The full-field DIC results showed the linear structural response of the NACRA F20c C-Foil. Moreover, a twist angle is captured for high wind speeds and angles of attack. The twist angle experienced in the wind tunnel appears to have small effects in sailing conditions (when the leeway angle is $\sim 2°$). However, due to the complex twist response experienced with increased forces, more studies should be performed to assess the change in angle of attack in water. The tip displacement was compared with the change in position of the tip vortex, evaluated with PIV. CFD simulations were performed to reproduce the wind tunnel experiment. This study was not only useful to validate the numerical simulations, but also to capture the response of the daggerboard under sailing forces.
From a sailor perspective, it is therefore possible to optimise the C-Foils positions in the daggerboard case, allowing a small positive pitch angle, especially to increase the vertical force component.

In order to maintain a high level of side force, it is possible to separate as much as possible the daggerboards from the centre of the catamaran.
It has to be noted however, that for a small leeway angle, the positive pitch of the board might be increased for better performances. Finally, further studies should be performed to assess the benefits in resistance of the relative increase in induced drag in flying condition compared to the increase in wetted area of the hull in standard catamaran configuration.

Acknowledgements

The authors would like to acknowledge the EPSRC for funding this research under grant number EP/009876/1. The authors would also thank the University of Southampton, especially the FSI group, the members of the TSRL and Dave Marshall and hit team in the R.J.Mitchell. Moreover, we would like to thank Dave Hollis from LaVision for his assistance in DIC and PIV and NACRA UK for supplying the tested foil.

References

[1] ISAF, “International NACRA 17 Class Rules,” NACRA, 2014.

[2] T. Zhengzong, L. Jin, X. Zhenzhong and G. Cheng, “Large Deformation Measurement Scheme for 3D Digital Image Correlation Method,” *Optics and Lasers in Engineering,* vol. 50, pp. 122-130, 2011.

[3] P. Rastogi and E. Hack, Optical Methods for Solid Mechanics: A Full-Field Approach, Wiley-VCH Verlag GmbH & Co., 2012.

[4] M. Sutton, J. Orteu and H. Schreier, Image Correlation for Shape Motion and Deformation Measurements: Basic Concepts, theory and applications, New York: Springer, 2009.

[5] P. Reu, “Stereo-Rig Design: Stereo-Angle Selection - Part 4,” *Experimental Techniques,* vol. 37, pp. 1-2, 2013.

[6] P. Reu, “Stereo-Rig Design: Creating the Stereo-Rig Layout - Part 1,” *Experimental Techniques,* vol. 36, pp. 3-4, 2012.

[7] X.-D. Ke, S. H.W., M. Sutton and Y. Wang, “Error Assessment in Stereo -Based Deformation Measurements,” *Experimental Mechanics,* vol. 51, pp. 423-441, 2011.

[8] J. Helm, S. McNeill and M. Sutton, “Improved Three-Dimensional Image Correlation for Surface

Displacement Measurement," *Optical Engineering*, vol. 35, no. 0091-3286/96/6.00, pp. 1911-1920, 1996.

[9] M. Raffel, C. Willert, S. Wereley and J. Kompenhans, Particle Image Velocimetry, 2007.

[10] Y.-J. Lee, Y.-T. Jhan and C.-H. Chung, "Fluid-Structure Interaction of FRP Wind Turbine Blades Under Aerodynamic Effect," *Composites*, 2012.

[11] R. Nicholls-Lee, S. Boyd and S. Turnock, "Development of High Performance Composite Bend-Twist Coupled Blades for a Horizontal Axis Tidal Turbine," in *17th International Conference on COmposite Materials*, Edimburgh, 2009.

[12] V. Fedorov, N. Dimitrov, C. Berggreen, S. Krenk, K. Branner and P. Berring, "Investigation of Structural Behavior due to Bend-Twist Couplings in Wind Turbine Blades," in *ICCM*, 2009.

[13] A. Maheri, S. Noroozi and J. Vinney, "Combined Analytical/FEA- Based Coupled Aero Structure Simulation of a Wind Turbine With Bend-Twist Adaptive Blades," *Renewable Energy*, vol. 32, no. 2007, pp. 916-930, 2006.

[14] J. Banks, L. Marimon Giovannetti, X. Soubeyran, A. Wright, S. Turnock and S. Boyd, "Assessment of Digital Image Correlation as a Method of Obtaining Defromations of a Structure Under Fluid Load," *Under Peer Review - Journal of Fluids and Structures*, 2014.

[15] R. Pemberton, S. Turnock, T. Doddl and E. Rogers, "A Novel Method for Identifying Vortical Structures," *Journal of Fluids and Structures*, vol. 16, no. 23, pp. 1051-1057, 2002.

[16] A. Philips and S. Turnock, "Application of the VORTFIND Algorithm for the Identification of Vortical Flow Features Around Complex Three-Dimensional Geometries," *International Journal for Numerical Methods in Fluids*, vol. 71, no. 11, pp. 1461-1474, 2013.

[17] OpenFOAM(R), "OpenFOAM-The Open Source CFD Toolbox - UserGuide, Version 2.01," 2011. [Online].

[18] J. Banks, L. M. Giovannetti, S. Turnock and S. Boyd, "Developing tools for assessing passive adaptive structures," in *Numerical Towing Tank Symposium (NuTTS)*, September 2014.